

Electrical Readout for Coherent Phenomena Involving Rydberg Atoms in Thermal Vapor Cells

D. Barredo, H. Kübler, R. Daschner, R. Löw, and T. Pfau

5. Physikalisches Institut, Universität Stuttgart, Pfaffenwaldring 57, 70550 Stuttgart, Germany

(Received 28 September 2012; published 21 March 2013)

We present a very sensitive and scalable method to measure the population of highly excited Rydberg states in a thermal vapor cell of rubidium atoms. We detect the Rydberg ionization current in a 5 mm electrically contacted cell. The measured current is found to be in qualitatively good agreement with a theory for the Rydberg population based on a master equation for the three-level problem, including an ionization channel and the full Doppler distributions at the corresponding temperatures. The signal-to-noise ratio of the current detection is substantially better than that of purely optical techniques.

DOI: [10.1103/PhysRevLett.110.123002](https://doi.org/10.1103/PhysRevLett.110.123002)

PACS numbers: 32.80.Rm, 03.67.Lx, 42.50.Gy

Coherent phenomena involving strongly interacting Rydberg atoms have recently led to the demonstration of first quantum devices such as quantum logic gates [1–3] and single-photon sources [4] based on ultracold atoms. All these experiments require precise control over the highly excited states' populations, which can be probed directly by field ionization [5,6] or by fluorescence techniques involving Rydberg shielding [7]. Since the strong van der Waals interaction has also recently been observed in vapor cells [8], scalable quantum devices based on the Rydberg blockade in above room temperature ensembles also seem to be within reach [9]. However, ion detectors such as electron multipliers or multichannel plates cannot be used in dense thermal vapors. For this reason, in thermal cells, most studies today use an indirect measurement of the excited state population by analyzing light fields leaving the atomic ensemble. Nevertheless, it is desirable to study not only the backaction of the vapor on the light, typically via electromagnetically induced transparency (EIT) [10], but also to directly measure the number of excited Rydberg states. One method, developed almost a century ago [11,12], makes use of thermionic diodes [13–15]. There, one of the electrodes is heated to emit electrons, which produce space charge limited gain for the amplification of ionized Rydberg atoms. The need of long ion trapping times requires large geometries for the space charge region (typically between 20 and 50 cm) and an additional shielded excitation region to minimize the effect of disturbing electric fields during excitation of the highly polarizable Rydberg atoms. Despite its high sensitivity, this drawback sets a practical limitation for further applications where size and scalability play a role. Direct detection of the ionization current produced in a gas by radiation fields constitutes the working principle of ionization chambers that are widely used in physics and has been successfully employed in ultrafast coherent spectroscopy of molecules [16]. In alkali vapors, direct detection of Rydberg ionization has been precluded, perhaps, by difficulties to distinguish truly gas phase effects from surface contributions in early works on photoionization [17] and

for the wide popularity and high sensitivity of thermionic diodes.

Here, we demonstrate that, in a symmetric configuration of atomic vapor between two transparent field plates, sizable currents in the nA regime directly reflect the Rydberg population and can be used as a probe with a very good signal-to-noise ratio. This opens unique possibilities to very efficiently probe small spectroscopic features involving Rydberg states in thermal vapor but also might be used to stabilize lasers. By extending this concept to an array of pixelwise arranged electrodes, high resolution spatial information on the Rydberg population can be obtained.

The experiments were performed with the setup schematically shown in Fig. 1. The Rb vapor is confined in a $l = 5$ mm electrically contacted cell which has been described in detail elsewhere [18]. In essence, it consists of two glass substrates glued to the edges of a glass frame attached to a reservoir tube. Two thin (approximately 5 nm) layers of Ni sputtered on the substrates act as field plates and provide electrical contact to the outside while still

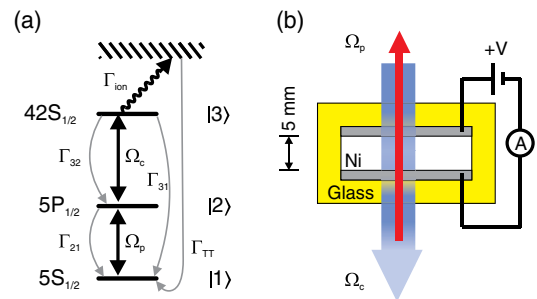


FIG. 1 (color online). (a) Three-level excitation scheme. The probe beam of Rabi frequency Ω_p couples the states $|1\rangle$ and $|2\rangle$, while the control laser of Rabi frequency Ω_c couples the states $|2\rangle$ and $|3\rangle$. (b) Experimental setup. The excitation takes place inside a glass cell filled with Rb vapor. Rydberg ions are detected as a current between two electrodes held at a slightly different electric potential V . The electrodes consist of 5 nm thin metallic layers of Ni which provide a 75% transparency for the excitation lasers.

allowing for a high (approximately 75%) optical transparency for the excitation lasers. Inside the cell, ^{85}Rb atoms are excited to a Rydberg state in a two-photon process in an EIT scheme [10]. A light field at $\lambda_p \sim 795$ nm of Rabi frequency Ω_p couples the $5S_{1/2} F = 3$ ground state and the $5P_{1/2} F' = 2$ intermediate state. In the second excitation step, a laser at $\lambda_c \sim 474$ nm populates the $42S$ Rydberg level. Both the probe and the coupling lasers cross the cell perpendicular to the field plates and overlap in the excitation region in a counterpropagating manner with beam waists ($1/e^2$ radii) $w_p = 0.16$ mm and $w_c = 0.51$ mm, respectively. Highly excited atoms are ionized mainly by collisions with other atoms, and the ionization products are detected as a current flow between the two electrodes, in which a low bias voltage (usually ~ 0.1 V) is applied. This low voltage does not significantly perturb the highly polarizable Rydberg atoms. The cell is enclosed in an electrostatically shielded oven, and both the temperature of the cell and the reservoir can be varied independently. The cell was always kept at a higher temperature with respect to the reservoir to avoid condensation of Rb on the glass surface, and the atom density is controlled by regulating the reservoir temperature. Finally, the transmission of the probe beam and the ionization current are measured simultaneously with a photodiode (Thorlabs DET36A) and a current amplifier (Keithley 427), respectively.

One of these measurements is shown in Fig. 2. It corresponds to a Stark map for the $42S$ Rydberg state, where the coupling laser is scanned around the two-photon resonance. The intensity of the coupling laser is modulated with an acousto-optic modulator, and the optical signal [Fig. 2(a)] is measured with a lock-in amplifier. The strength of the electric field is controlled by ramping the voltage applied directly to the electrodes. The corresponding ionization current signal is shown in Fig. 2(b), after background subtraction. This background is mainly due to photoelectrons produced by the 474 nm light on the Ni electrodes, whose work functions are lowered by adsorbed Rb atoms on the surfaces. In the optical signal, the EIT peak is clearly observed for low electric fields but broadens and is hardly observable for fields higher than 10 V/cm. In contrast, the ionization current produces a map with a higher contrast in which the Rydberg signal can be followed over the full range of the measurement, despite broadening. The second feature starting at a Stark shift of $\sim -250 \times 2\pi$ MHz corresponds to Rydberg excitation from the Doppler-allowed $5P_{1/2} F' = 3$ hyperfine state [19], which is barely visible in the EIT signal. We have not found an explanation for the third weak dispersive line starting at $\sim 150 \times 2\pi$ MHz. We have observed similar features in both optical and electrical domains in Stark maps recorded with longer cells and that may arise, presumably, from backreflections of the lasers inside the cell. The inset of Fig. 2(b) shows the behavior of the signal at low electric fields. Both signal and background vanish at 0 V because a finite bias voltage is

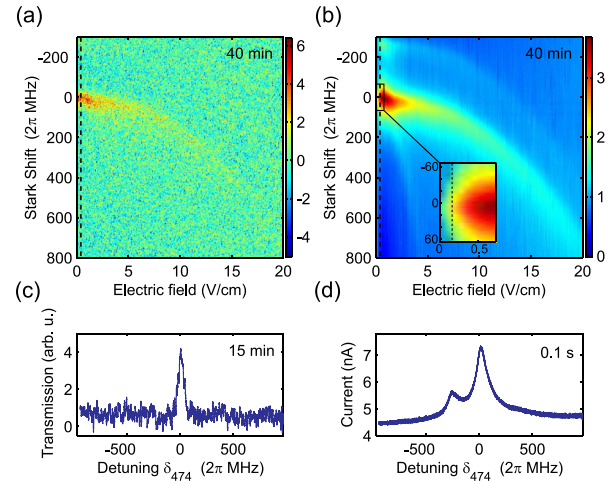


FIG. 2 (color online). Stark maps of the $42S$ Rydberg state. Transmission of (a) the probe field and (b) the ionization signal, measured simultaneously, after background subtraction. The inset shows an enlarged area at a low electric field. (c) Averaged optical signal measured with a lock-in amplifier and (d) the corresponding single-shot ionization signal recorded 9000 times faster.

needed to detect the current. In our conditions, the ion or electron collection efficiency is fully saturated at around 0.5 V. Such a low optical signal may be surprising if compared to that obtained with longer vapor cells, and, therefore, it is worth stressing that similar signal-to-noise ratios have been reported for this type of cell [18], where peak heights are further reduced by pressure broadening ($\sim 50 \times 2\pi$ MHz). The striking difference in the signal-to-noise ratio between the optical and the ionization signals is better seen in a cut at a constant electric field. In Fig. 2(c), the measured EIT peak (of width $\sim 55 \times 2\pi$ MHz) at a field of 0.4 V/cm was averaged over 90 traces at a scanning rate of 100 mHz, with an integration time constant of 3 ms. In comparison, the ionization signal, shown in Fig. 2(d), was obtained in a single shot with the coupling laser scanning at 10 Hz and a rise time constant of the current amplifier of $10 \mu\text{s}$. The width of the peaks is around $\sim 120 \times 2\pi$ MHz. It is important to distinguish between the measurement of the current and the transmission of the probe laser, which provide access to two different observables, namely, the population of the upper state and the coherence in the lower transition. Therefore, both signals cannot be directly compared. In a Stark map, measuring ions is experimentally more favorable because ionization signals can in principle be extracted from an essentially zero background, in contrast to optical detection. In practice, in this excitation scheme, electrons produced by a photoelectric effect and two-photon Rb ionization signals contribute to the observed background and set the ultimate limit to which noise can be reduced [15].

To demonstrate that this electrical current is a direct measure of the population of the $42S$ state, ionization

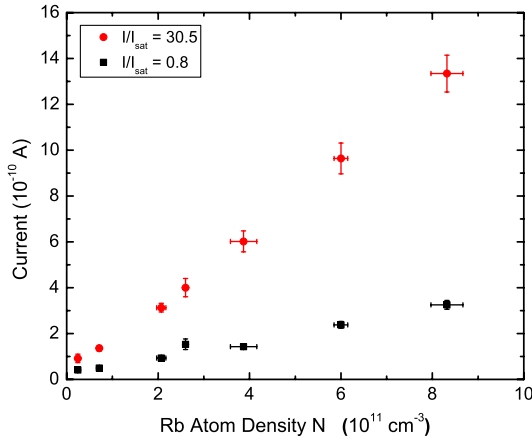


FIG. 3 (color online). Scaling of the measured ionization signal with ground state density for two different probe laser intensities $I = 0.8I_{\text{sat}}$ and $30.5I_{\text{sat}}$. The applied voltage is 0.75 V. The error bars represent ± 1 standard deviation confident intervals.

spectra were first measured as a function of Rb vapor density for various probe laser intensities (Fig. 3). For each point, the atom density N was estimated from control absorption measurements and peak heights were extracted from fittings to Lorentzian profiles. Figure 3 shows a linear scaling for $N > 2 \times 10^{11} \text{ cm}^{-3}$, indicating that the probability that a Rydberg atom gets ionized in a collision stays constant. This is the expected behavior if the collisional ionization rate Γ_{ion} exceeds the sum of the rates of all nonionizing decay channels. We have ruled out surface ionization as the origin of the detected current. Surface ionization should produce a velocity selection and subsequently an asymmetry in the Doppler profile distribution as a consequence of the geometrical arrangement. Such an asymmetry was not observed. Photoionization due to the 474 nm light was also discarded because the signal was not observed to increase if a third strong nonresonant 480 nm laser is added. Also, ionization rates by blackbody radiation are expected to be very small [20]. Collision with electrons should also play a minor role in ionization, as judged from experimental ionization cross sections [21], which lead to an upper limit for ionization in our conditions of about 5 kHz. This is further supported by the fact that an increase of the nonresonant light intensity increases the current background but does not produce higher signals.

The next step was to investigate the behavior of the signal as a function of laser power. To do so, we performed a simulation based on the analytical solution of the Lindblad equation in a steady state, in which all coupling strengths and detunings are included as fixed parameters:

$$\dot{\rho} = -\frac{i}{\hbar}[\hat{H}, \hat{\rho}] + \hat{L}(\rho) = 0, \quad (1)$$

with the Hamilton operator

$$\hat{H} = \hbar \begin{pmatrix} 0 & \frac{1}{2}\Omega_p & 0 & 0 \\ \frac{1}{2}\Omega_p^* & -\delta_p & \frac{1}{2}\Omega_c & 0 \\ 0 & \frac{1}{2}\Omega_c^* & -\delta_p - \delta_c & 0 \\ 0 & 0 & 0 & 0 \end{pmatrix},$$

where Ω_p , Ω_c , δ_p , and δ_c are the probe and coupling Rabi frequencies and energy detunings, respectively. The velocity distribution of the atoms is taken into account by their Doppler shift $\delta_{v,i} = \vec{k}_i \times \mathbf{v}$ for each transition, weighted by a 1D Boltzmann distribution $g_v = \sqrt{m/(2\pi k_B T)} \exp[-mv^2/(2k_B T)]$. The Lindblad operator $\hat{L}(\rho)$ includes the decays Γ_{ij} as depicted in Fig. 1, where the ionization channel is essentially treated as a fourth level with $\Gamma_{34} = \Gamma_{\text{ion}}$, and the cycle is closed with the transit-time rate $\Gamma_{\text{TT}} = 0.25 \times 2\pi \text{ MHz}$, estimated from the beam waist w_p and the average atom velocity at a mean cell temperature of $\sim 70^\circ \text{C}$ [22]. The ionization rate was estimated from the observed width of the EIT signal to be $\Gamma_{\text{ion}} = 50 \times 2\pi \text{ MHz}$. This is consistent with measurements performed in similar cells [18] and presumably comes from pressure broadening due to contaminants inherent to these glued-type vapor cells.

The comparison between the theoretical calculation and the experimental results is summarized in Fig. 4. The scaling behavior of the current with both the probe (a) and coupling laser (b) Rabi frequencies is shown. Each dashed line represents the calculated population scaled with a prefactor. The Rabi frequencies were estimated from the beam waists at the excitation region and the incident laser power. No further correction was made due to the attenuation of the radiation in the vapor. For this reason, only the low density curves are shown. In these conditions, and since most Rabi frequency values in Fig. 4(a) correspond to probe intensities much higher than the saturation intensity of the $5S_{1/2} - 5P_{1/2}$ transition, the propagation effects are expected to be small. For higher densities, propagation of the light field in the optically thick medium must be included in the model [23], and the experimental data depart from the prediction of our simple model. A good agreement is found in both data sets, demonstrating that the measured ionization signal can be directly correlated with the Rydberg state population. A rough check for the order of magnitude of the prefactors used to scale the Rydberg population to the measured current can be obtained from our simulation. The highest current value in Fig. 4(a) of $\sim 5 \times 10^{-10} \text{ A}$ ($\Omega_p \sim 180 \times 2\pi \text{ MHz}$, $\Omega_c \sim 0.45 \times 2\pi \text{ MHz}$) corresponds to a steady state population of the Rydberg level $\rho_{33} \sim 4 \times 10^{-6}$, including Doppler averaging over the velocity classes. The expected current from the experimental parameters, i.e., the ionization volume ($l \times \pi w_p^2$), the $5S_{1/2} F = 3$ ground state atom density ($N_g = 9.4 \times 10^{10} \text{ cm}^{-3}$), and assuming $\Gamma_{\text{ion}} = 50 \times 2\pi \text{ MHz}$ as the Rydberg production

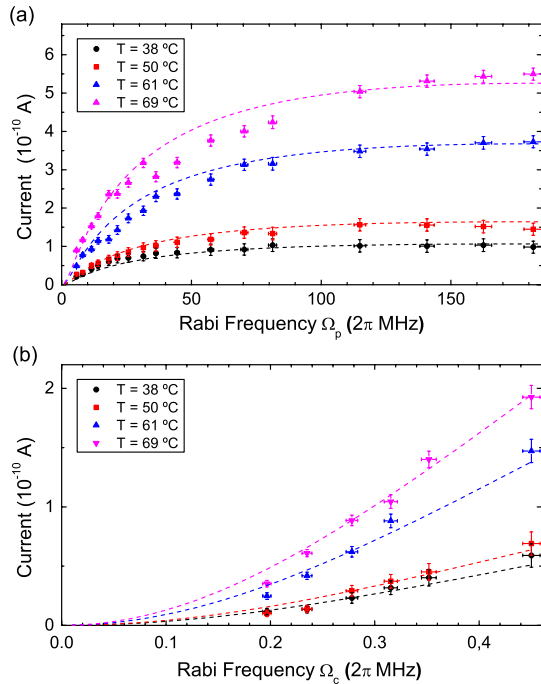


FIG. 4 (color online). Measured ionization signal as a function of the peak probe field Rabi frequency Ω_p (a) at a fixed coupling Rabi frequency $\Omega_c = 0.45 \times 2\pi$ MHz and (b) at a coupling laser peak Rabi frequency Ω_c at $\Omega_p = 14 \times 2\pi$ MHz for different ground state atom densities. The dashed lines are theoretically calculated Rydberg state populations scaled to the corresponding atomic density. The error bars represent ± 1 standard deviation confident intervals.

rate, yields a value of about 8 nA, which is about a factor of 10 higher than what we measure. The assignment of a decay rate from the measured width of the EIT signal assumes broadening as only due to ionizing collisions. However, other mechanisms such as dephasing, not necessarily leading to ionization, can also broaden the EIT profile. An overestimation of the number of ionizing collisions could explain this discrepancy. Other processes not included in the model could also be the origin of a larger current signal width ($\sim 120 \times 2\pi$ MHz) compared to the optical signal. In experiments performed in continuously pumped vapor cells, both current and EIT widths were found to be smaller and comparable for the same laser intensities, excluding saturation effects like power broadening. A gain mechanism due to space charge limitation or avalanche ionization in the medium is not evident.

In conclusion, we have shown that the measurement of the Rydberg ionization current in thermal vapor cells provides, over a wide range of densities and laser powers, a direct measure of Rydberg state population. Since the Rydberg blockade fraction and the probe beam optical susceptibility are coupled by a simple universal relation [24], the combination of EIT spectroscopy with the measurement of the ionization current represents a promising

approach to study the interaction effects between Rydberg atoms in a thermal environment [25]. This method is not only well suited for applications in quantum information processing based on the blockade of the Rydberg population but also enables applications in precision spectroscopy (e.g., to measure electric fields near surfaces [26] or in free space [27]) and laser stabilization. Moreover, spatial resolution and scalability are possible, as the electrodes can be structured similarly to the way it is done in display technology and Rydberg atoms can be excited in much smaller vapor cells [28].

We acknowledge helpful discussions with J. P. Shaffer. We thank E. Kurz and N. Frühauf for assistance in the construction of the cell and E. Schöll for additional data integrity checks. This work was supported by a Marie Curie Intra European Fellowship (No. 272831) within the 7th European Community Framework Programme, by the ERC under Contract No. 267100 and BMBF within QuOReP (Project No. 01BQ1013). We also acknowledge the financial support of the Future and Emerging Technologies (FET) Programme within the Seventh Framework Programme for Research of the European Commission, under FET-Open Grant MALICIA (No. 265522).

-
- [1] A. Gaetan, Y. Miroshnychenko, T. Wilk, A. Chotia, M. Viteau, D. Comparat, P. Pillet, A. Browaeys, and P. Grangier, *Nat. Phys.* **5**, 115 (2009).
 - [2] E. Urban, T. A. Johnson, T. Henage, L. Isenhower, D. D. Yavuz, T. G. Walker, and M. Saffman, *Nat. Phys.* **5**, 110 (2009).
 - [3] L. Isenhower, E. Urban, X.L. Zhang, A.T. Gill, T. Henage, T. A. Johnson, T. G. Walker, and M. Saffman, *Phys. Rev. Lett.* **104**, 010503 (2010).
 - [4] Y. O. Dudin and A. Kuzmich, *Science* **336**, 887 (2012).
 - [5] T. F. Gallagher, *Rydberg Atoms* (Cambridge University Press, Cambridge, England, 2005).
 - [6] T. Vogt, M. Viteau, A. Chotia, J. Zhao, D. Comparat, and P. Pillet, *Phys. Rev. Lett.* **99**, 073002 (2007).
 - [7] P. Schauf, M. Cheneau, M. Endres, T. Fukuhara, S. Hild, A. Omran, P. Pohl, C. Gross, S. Kuhr, and I. Bloch, *Nature (London)* **491**, 87 (2012).
 - [8] T. Baluktsian, B. Huber, R. Löw, and T. Pfau, *Phys. Rev. Lett.* **110**, 123001 (2013).
 - [9] R. Löw and T. Pfau, *Nat. Photonics* **3**, 197 (2009).
 - [10] A. K. Mohapatra, T. R. Jackson, and C. S. Adams, *Phys. Rev. Lett.* **98**, 113003 (2007).
 - [11] K. H. Kingdon, *Phys. Rev.* **21**, 408 (1923).
 - [12] G. Hertz, *Z. Phys.* **18**, 307 (1923).
 - [13] K. C. Harvey and B. P. Stoicheff, *Phys. Rev. Lett.* **38**, 537 (1977).
 - [14] K. Niemax, *Appl. Phys. B* **38**, 147 (1985).
 - [15] P. Herrmann, N. Schlumpf, V. Telegdi, and A. Weis, *Rev. Sci. Instrum.* **62**, 609 (1991).
 - [16] R. Uberna, Z. Amitay, C. X. W. Qian, and S. R. Leone, *J. Chem. Phys.* **114**, 10311 (2001).
 - [17] R. C. Williamson, *Phys. Rev.* **21**, 107 (1923).

- [18] R. Daschner, R. Ritter, H. Kübler, N. Frühauf, E. Kurz, R. Löw, and T. Pfau, *Opt. Lett.* **37**, 2271 (2012).
- [19] Note that, due to different Doppler velocity class selections by the probe and coupling lasers, the hyperfine splitting of the $5P_{1/2}$ is scaled by the factor $(\lambda_p/\lambda_c - 1)$.
- [20] I. I. Beterov, D. B. Tretyakov, I. I. Ryabtsev, V. M. Entin, A. Ekers, and N. N. Bezuglov, *New J. Phys.* **11**, 013052 (2009).
- [21] P. Kashtanov, M. Myasnikov, and B. Smirnov, *J. Exp. Theor. Phys.* **108**, 18 (2009).
- [22] J. Sagle, R. K. Namiotka, and J. Huennekens, *J. Phys. B* **29**, 2629 (1996).
- [23] J. Vanier, M. W. Levine, D. Janssen, and M. Delaney, *Phys. Rev. A* **67**, 065801 (2003).
- [24] C. Ates, S. Sevincli, and T. Pohl, *Phys. Rev. A* **83**, 041802 (2011).
- [25] S. Sevincli, C. Ates, T. Pohl, H. Schempp, C. S. Hofmann, G. Günter, T. Amthor, M. Weidemüller, J. D. Pritchard, D. Maxwell, A. Gauguet, K. J. Weatherill, M. P. A. Jones, and C. S. Adams, *J. Phys. B* **44**, 184018 (2011).
- [26] A. Tauschinsky, R. M. T. Thijssen, S. Whitlock, H. B. van Linden van den Heuvell, and R. J. C. Spreeuw, *Phys. Rev. A* **81**, 063411 (2010).
- [27] A. K. Mohapatra, M. G. Bason, B. Butscher, K. J. Weatherill, and C. S. Adams, *Nat. Phys.* **4**, 890 (2008).
- [28] H. Kübler, J. P. Shaffer, T. Baluktisian, R. Löw, and T. Pfau, *Nat. Photonics* **4**, 112 (2010).